


**Ray tracing with quantum correlated photons to image a three-dimensional scene**Yingwen Zhang <sup>1</sup>, Antony Orth,<sup>1</sup> Duncan England,<sup>1,\*</sup> and Benjamin Sussman<sup>1,2</sup><sup>1</sup>*National Research Council of Canada, 100 Sussex Drive, Ottawa, Ontario K1A0R6 Canada*<sup>2</sup>*Department of Physics, University of Ottawa, Ottawa, Ontario K1N 6N5, Canada*

(Received 1 September 2021; accepted 15 December 2021; published 3 January 2022)

To capture a three-dimensional (3D) image, conventional methods often require multiple two-dimensional images of the scene from different perspectives. Here we show the reconstruction of a 3D scene with a fixed camera using quantum correlated photon pairs from a single source. Correlated photon pairs are effectively mirror images of each other so, by measuring the emission position of one photon, and the emission angle of the other, the entire propagation trajectory of the pair, and, subsequently, the 3D scene, can be reconstructed. The high photon correlation and low photon flux from a quantum source also makes it well suited for 3D imaging of light sensitive samples.

DOI: [10.1103/PhysRevA.105.L011701](https://doi.org/10.1103/PhysRevA.105.L011701)

A grand challenge of quantum photonics is to develop techniques that use photons with nonclassical statistics to go beyond the capabilities of classical approaches. There has been nascent success in the development of two-dimensional (2D) imaging techniques, such as sub-shot-noise imaging, quantum illumination, and quantum ghost imaging [1–4]. In these techniques, significant noise reduction can be achieved under low photon illumination conditions through the utilization of the strong correlations in one of more of the many degrees of freedom (DOF) between entangled photon pairs, such as time, polarization, position/momentum, frequency, etc. Usually both photons from the pair are measured in the same DOF, and the correlations are used, for example, to remove noise either from background light (quantum illumination) or from shot noise (sub-shot-noise imaging). Alternatively, at the expense of noise reduction, each photon can be measured in a different DOF with the DOFs chosen such that they are complimentary to each other to unlock new imaging capabilities. Building upon prior techniques, in this Letter, we use time-correlation measurements to first identify the photon pairs and concurrently measure the position of one photon and the momentum of its partner. By utilizing the inherent position and momentum correlations between the photons, we can reconstruct the full propagation trajectory of every photon pair and go on to use this information to realize three-dimensional (3D) scene reconstruction.

In conventional optical imaging, only the 2D spatial distribution of light on the camera or detector is recorded. By capturing multiple 2D images from different perspectives, both position and angular information of the light rays can be gained, thus, 3D information of the scene can be reconstructed. This allows capabilities, such as refocusing, depth of field adjustments, and parallax viewing of the scene to be performed, all in postprocessing. One way to achieve this is

through a moving light source, such as in Fourier ptychography [5,6] whereby a sample is scanned at different angles by light emitted from individual elements of a light-emitting diode array. Alternatively, with a fixed light source, cameras can be placed at different locations or angles relative to the scene, such as in axially distributed sensing [7] where the camera is moved relative to the subject or vice versa. An alternative technique that requires no moving parts, and only a single camera is known as plenoptic or light field imaging [8,9]. In this approach, a microlens array is placed one focal length away from a CCD sensor, each microlens illuminates a subset of the pixels in the CCD. By knowing which lens the light ray enters and onto which pixel it, subsequently, focuses, one can obtain both position and angular information of the light ray, respectively. Plenoptic imaging is akin to imaging a scene simultaneously with an array of cameras, thus, requires no scanning or moving parts. This class of 3D imaging techniques of placing camera(s) at different angles relative to the scene is also known as integral imaging [10,11]. A multitude of research in applications using these techniques has been performed in recent decades, to name a few, and this includes target recognition [12,13], microscopy [6,14–16], particle tracking [17,18], wave-front sensing [19–21], and microendoscopy [22].

Due to the way these conventional techniques are performed, they tend to have a relatively low angular resolution compared to their position resolution as a result of the number of viewing angles limited by either the number of light sources or camera placement locations. And in the case of plenoptic imaging, position resolution has to be sacrificed for angular resolution. To overcome these limitations, the use of temporally and spatially correlated classical or quantum light has been proposed [23–25] where one beam illuminates a scene to obtain position information, and the momentum/angular information of the correlated partner beam is measured on a separate sensor. In this way, both position and momentum can be measured with high resolution allowing larger depth of fields and more parallax viewing angles. This

\*duncan.England@nrc-cnrc.gc.ca

technique, termed *correlation plenoptic imaging* (CPI) has been demonstrated using weakly correlated thermal light [26,27], but further advantages have been predicted using highly correlated quantum light [24]. The strength of the correlation between two beams can be quantified by the degree of second-order coherence  $g^{(2)}$  where classical light is bound by  $g^{(2)} \leq 2$ . Quantum light sources have been demonstrated to exhibit  $g^{(2)}$  in excess of 100 so the signal-to-noise ratio in CPI can potentially be orders of magnitude higher using quantum light compared to classical light of the same intensity [28]. A similar approach using quantum correlated light has also been used to demonstrate Fourier ptychography for amplitude and phase imaging [29]. Here, an intensified CCD camera triggered by a single-photon avalanche detector (SPAD) sensor is used to acquire the data with the SPAD scanned across the Fourier plane of the source.

Based on the proposal in Ref. [24], here, we demonstrate the reconstruction of a scene's 3D information through ray tracing using quantum correlated photon pairs for which we will term *quantum correlation plenoptic imaging* (QCPI). QCPI actually shares similarities with both conventional plenoptic imaging and Fourier ptychography, but also has important differences. QCPI uses quantum correlated photon pairs generated through the process of spontaneous parametric down-conversion (SPDC) with the aid of a time-tagging camera, capable of time tagging every photon detection with nanosecond precision. By imaging one photon in the crystal's Fourier plane and its partner photon in the crystal image plane, then taking advantage of the strong time, position, and momentum correlation properties of the SPDC photon pairs, we were able to trace the propagation trajectory of all the detected photon pairs. Just as in plenoptic imaging, no scanning or moving parts are required to measure the photon trajectories, although here, the position and momentum measurement comes from the quantum correlation rather than through a microlens array. QCPI is also similar to Fourier ptychography in the sense that each photon is illuminating the scene from a different angle, but the illumination randomly changes due to the stochastic nature of quantum light, thus, separate light sources are not required. In our proof-of-principle demonstration, we show that QCPI can achieve various 3D imaging capabilities, such as refocusing, depth-of-field adjustments, and parallax viewing of a scene all at a very low photon flux of  $\sim 1000$  photons per second per pixel (or  $5 \times 10^{-11}$  W/cm<sup>2</sup> on the sample).

*Experimental setup and method.* The experimental setup is shown in Fig. 1. A 405-nm continuous wave (CW) laser is used to pump a 1-mm-thick Type-II ppKTP crystal to produce 810 nm, orthogonally polarized photon pairs correlated in time, position, and momentum through the process of SPDC. A long-pass spectral filter placed directly after the crystal is used to block out the 405-nm pump and let through the 810-nm SPDC photons. As the SPDC photons are emitted from the crystal in a divergent manner, a 100-mm lens is used to collimate the SPDC beam. Thereafter a polarizing beam splitter (PBS) is used to split the photon pairs into separate paths in which the sample to be imaged is placed in one of the paths. The two photon beams are then recombined but slightly displaced by a second PBS just before the time-tagging camera (TPX3CAM [30,31]) such that each beam will be imaged

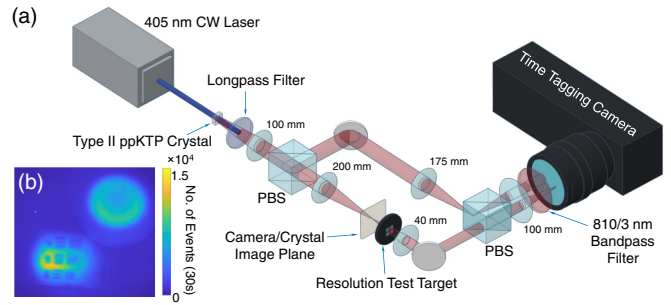


FIG. 1. (a) Schematic of the QCPI setup. (b) Raw image taken over 30 s before any postprocessing captured on the TPX3CAM with the resolution target placed 4 mm off focus.

onto different locations of the camera. In one path, through two magnifying  $4f$  imaging systems, the crystal plane is first imaged onto the location at which the sample is to be placed and then onto the camera with the beam spot magnified five times. In the other path, three lenses are used such that the Fourier plane of the crystal is imaged onto the camera with a slightly demagnified beam spot. Ideally, two cameras can be used, one for each beam spot to achieve higher position and momentum resolution. Compared to using a frame-based camera, the event-driven time-tagging camera significantly simplifies our setup as no scanning elements, or an image preserving delay line is required.

A thin (1-mm) nonlinear crystal is used to reduce the uncertainty in the depth at which the SPDC photons are generated inside the crystal, and this will improve the photon pair's position correlation. Also, since the SPDC photon pairs' wavelengths are not necessarily degenerate, uncertainties in their momentum correlation will be introduced. To reduce this uncertainty and to reduce background light, a 810/3-nm spectral bandpass filter is placed just before the camera.

The power of the UV laser has been attenuated down to 20 mW, generating a total of approximately  $1.3 \times 10^7$  photon pairs per second or an average photon flux of  $\sim 1000$  photons per pixel per second (after accounting for the system quantum efficiency of 4%). Increasing the pump beam power will produce more SPDC photons, thereby speeding up the data-acquisition process, however, at the cost of reduced spatiotemporal correlation between the photons, thereby introducing more noise in the images. This is due to the increased likelihood of multiphoton pair production in the crystal during a detection time window, thus, causing the incorrect photons being identified as a pair during time-correlation analysis. Inversely, by reducing the pump power, one can reduce the image noise but at the cost of longer data-acquisition time.

In postprocessing, a virtual circular aperture is placed around each beam in the images in order to limit time-correlation analysis to just the photons within the two beams, thus, reducing noise. Time-correlation analysis is then performed on all photons detected between the two selected beam spots to identify the SPDC photon pairs. Finally, by utilizing the property that the photon pairs are perfectly correlated in position and anticorrelated in momentum, and the fact that all the optical elements and distances between them are known,

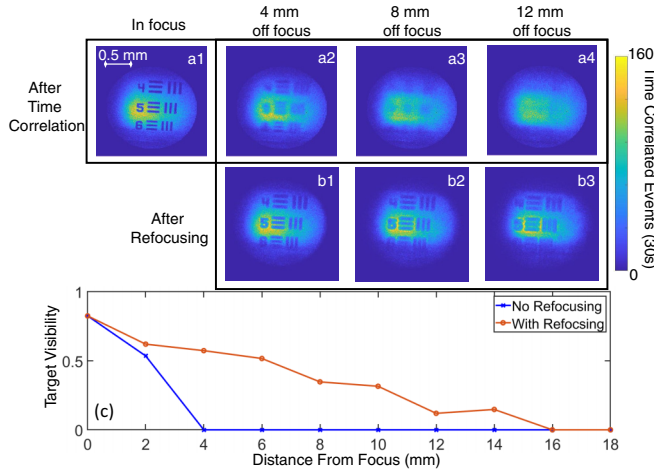


FIG. 2. Demonstration of image refocusing in QCPI using a 1951 USAF resolution test target placed at different distances from the focal plane of the imaging lenses. The line sets has a spacing of approximately five line pairs per millimeter. The images in (a) from a1–a4 are the images obtained after performing only time-correlation measurements on the detected photons with a1 as the ground truth of the resolution test target when placed in focus. (b) From b1–b3, are images obtained after refocusing is performed in postprocessing on a2–a4, respectively. The degradation of the visibility before and after refocusing of the three bars in the target with respect to their distance to the focus is plotted in (c). The data-acquisition time for each image is 30 s. Refocused image of all distances shown in (c) can be found in the Supplemental Material [33].

we can make use of the Klyshko picture [32] to backtrack the propagation path of one photon from its near field to the far field of the other or vice versa, treating the crystal as a mirror and gain both the position and the momentum information of the photon pairs. Since the system is still mostly paraxial (the maximum illumination angle on our sample is  $\sim 1.5^\circ$ ), the trajectory of the photons can be determined through a simple ray transfer-matrix analysis,

$$\begin{bmatrix} \vec{r}_2 \\ \vec{\theta}_2 \end{bmatrix} = \begin{bmatrix} A & B \\ C & D \end{bmatrix} \begin{bmatrix} \vec{r}_1 \\ \vec{\theta}_1 \end{bmatrix}, \quad (1)$$

where  $\vec{r}_1$  and  $\vec{r}_2$  are the positions of each photon pair detected at the two camera image planes,  $\vec{\theta}_1$  and  $\vec{\theta}_2$  are the angles at which the photons hits each plane and the ray transfer ( $ABCD$ ) matrix is determined by the optical components placed between the two image planes. Since  $\vec{r}_1$  and  $\vec{r}_2$  are known from the raw image data taken by the two cameras and the  $ABCD$  matrix is also known,  $\vec{\theta}_1$  and  $\vec{\theta}_2$  can be easily determined from Eq. (1). Thus, the full propagation trajectory of every detected photon pair is known, and with this information, one can perform in postprocessing, the refocusing, depth of field adjustments, and parallax viewing of the scene. More details on the camera and data processing can be found in the Supplemental Material [33].

**Experimental results.** In Fig. 2, the refocusing capability of QCPI is demonstrated on images taken of a 1951 USAF resolution test target placed at different distances from the focal plane of the imaging lenses. It can be seen that when the target is placed 4 mm away from the focus, in a conventional

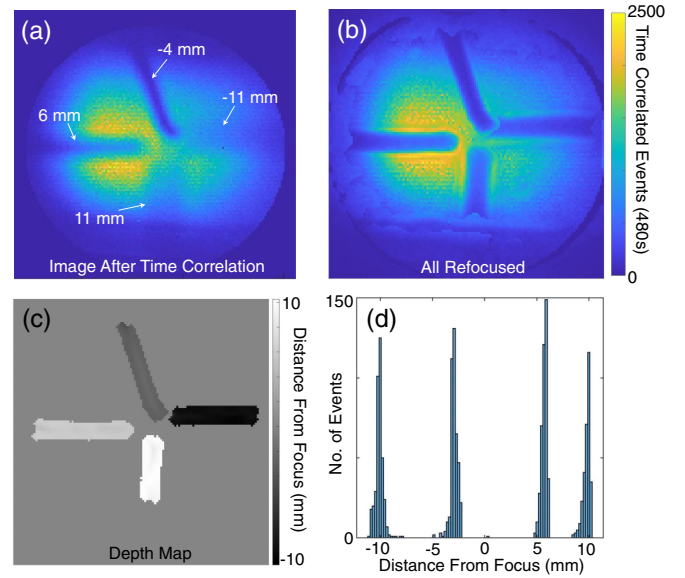


FIG. 3. Images demonstrating the refocusing and depth reconstruction of four thin wires of 0.15-mm diameter placed at different distances from the focus. (a) Raw image of the four wires after performing time-correlation measurements with the manually measured distance from the focus shown on image. (b) All wires brought to focus through post processing. (c) Depth map of the wires with the histogram of the depth shown in (d).

image [Fig. 2(a2)], the bars in the resolution target can no longer be clearly observed, however, through QCPI they can be brought back into focus [Fig. 2(b1)] with good image sharpness. Even at extreme distances where features of the resolution target can no longer be identified through conventional imaging [Fig. 2(a4)], QCPI can still bring the image mostly back into focus [Fig. 2(b3)]. In Fig. 2(c), we show the degradation in the visibility before and after refocusing of the three central horizontal bars (to the right of number “5,” approximately  $160 \mu\text{m}$  apart) with respect to the distance the resolution target is placed away from the focus. The visibility is defined as  $\frac{I_{\text{max}} - I_{\text{min}}}{I_{\text{max}} + I_{\text{min}}}$ , where  $I_{\text{min}}$  is the average intensity for the dark bars and  $I_{\text{max}}$  is the average intensity for the bright region between the bars. When there are no visible troughs between intensity peaks in the cross section of the bars, the visibility is then set to 0. The range over which the lines are resolvable (nonzero visibility) increases from 4 to 16 mm through refocusing. The sharpness of the refocusing deteriorates when the target is placed further away from the focus, and this may be due to a multitude of factors, such as limited position and momentum resolution, imperfect position correlation caused by the finite thickness of the crystal introducing uncertainties over the depth at which the photon pairs are generated, and lastly, imperfect momentum anticorrelation caused by the photon pairs having nondegenerate wavelength and pump beam divergence at the crystal. The affect these factors have on QCPI will require further more detailed investigation in the future and are not within the scope of this Letter.

In Fig. 3, we show the refocusing and a depth map of four thin wires of 0.15-mm diameter placed at different depths within the beam. Figure 3(a) shows the traditional image of the scene after time correlation without momentum filtering.

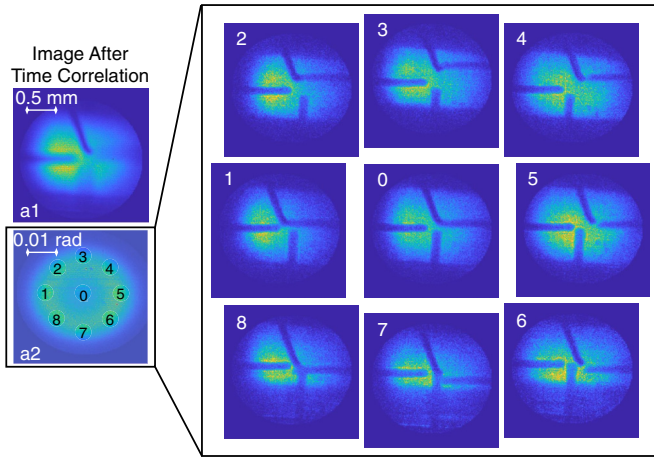


FIG. 4. Images demonstrating parallax visualization and depth-of-field enhancement on four thin wires placed at different depth from the focus. a1 and a2 show the raw images taken in the crystal plane and its Fourier plane, respectively, after time-correlation analysis. To demonstrate parallax viewing, correlation events between the full crystal plane and nine subregions of the Fourier plane (as indicated in a2) were selected out. Each subregion of a2 corresponds to a different viewing angle of the wires, and these are displayed as a set of nine images, labeled 0–8, displayed on the right, each corresponding to the nine labeled subregions (illumination and viewing angles) in a2, respectively. Due to the small diameter, i.e., small momentum spread of each of the subregions, an increase in the depth of field is also achieved. The diameter of each subregion is 20-pixels wide with the diameter of the virtual aperture around the full beam at 130 pixels. The raw image data were acquired over 8 min to ensure enough photons are accumulated within each subregion. Smaller subregions can potentially be used but will require substantially longer data-acquisition times.

Using the photon momentum information, this image is refocused into a stack of images, each corresponding to a different focus plane. The depth map in Fig. 3(c) is obtained by choosing the sharpest refocused plane for each pixel in the image [34]. Good agreement is achieved between the reconstructed depth and the manually measured depth [Fig. 3(d)]. The slight discrepancy is likely due to inaccuracies in manually measuring with a ruler the wire locations and the distances between the optical components (lenses, mirrors etc.). This measurement inaccuracy, however, does not affect the image sharpness in refocusing as any inaccuracies here is a global effect affecting all photons in the same manner, thus, it will only introduce errors in parameters, such as the size and position of the sample. From this depth map, an all-in-focus image is constructed in Fig. 3(b) by modifying the refocus position to the depth map value in Fig. 3(c) on a per-pixel basis. More details on how the depth mapping is performed can be found in the Supplemental Material [33]. The demonstration of depth-of-field enhancement and parallax visualization on the four wires is shown in Fig. 4. By selecting coincidence events from a smaller subregion on the Fourier plane, we can limit the allowed photon momentum, thus, adjusting, in post-processing, the imaging depth of field in the corresponding crystal image plane. Choosing small subregions off center from the optical axis results in the Fourier plane beam re-

sults in viewing the wires on the crystal image plane from different angles, thus, allowing parallax visualization to be performed.

It is important to note that QCPI does not necessarily require the sample to be placed near the image plane of the crystal; one can have the sample placed on the crystal's Fourier plane and still perform QCPI. As the beam is more collimated and larger on the Fourier plane, it will be more suited for imaging larger objects with more depth. Demonstration of this is shown in the Supplemental Material [33]. Videos demonstrating the postprocessing of refocusing, depth-of-field adjustments, and parallax viewing are also shown in the Supplemental Material [33].

*Conclusion.* To conclude, in this proof-of-concept demonstration of QCPI, we have demonstrated some of the major capabilities of 3D imaging, including refocusing, depth-of-field adjustments, and parallax visualization of an object and scene. QCPI shares similarities with both plenoptic imaging and Fourier ptychography. QCPI requires no scanning or moving parts to capture information on the photon trajectories in which it shares similarity with plenoptic imaging. However, in the Klysko picture where the photon trajectory is backtracked from the crystal's Fourier plane to the image plane, the similarities lies with Fourier ptychography in which each pixel of the Fourier plane camera can be treated as a light source that randomly emits photons.

QCPI exhibits conceptual advantages over conventional 3D imaging, and this initial demonstration takes significant steps toward realizing these advantages. In particular, the momentum, angle, and position of the photon can be measured with high resolution. In conventional techniques, the position is typically measured by a high-resolution camera, but angular resolution is limited by the number of camera positions (integral imaging), the number of light sources (Fourier ptychography), or the pitch of the microlens array (plenoptic imaging). In QCPI, the momentum resolution is only limited by the number of pixels in the camera placed on the Fourier plane and the photons' degree of momentum correlation, also, unlike in plenoptic imaging, one does not need to sacrifice imaging pixels to measure angular information. Here around  $10^4$  pixels were used, but with new high-resolution time-tagging cameras [35], this could increase to  $10^6$  in the near future. Therefore, with a single quantum light source, one could potentially illuminate a 3D scene from  $10^6$  different angles (this, of course, would also depend on other factors, such as the degree of position and momentum correlation between the photon pairs and the diffraction limit of the system), a goal that is impractical with conventional techniques.

Since QCPI is based on quantum photon correlations, it also gains some of the advantages of quantum correlation imaging over classical correlation imaging techniques. As a result of the sub-Poissonian photon statistics of the SPDC photons giving a much higher second-order photon correlation compared to classical sources of the same intensity, a much lower background noise can be theoretically obtained using SPDC photons in correlation imaging under low illumination conditions [36,37]. This makes QCPI potentially well suited for imaging light sensitive samples, such as the retina cells in human and animal eyes, and we expect other advantages

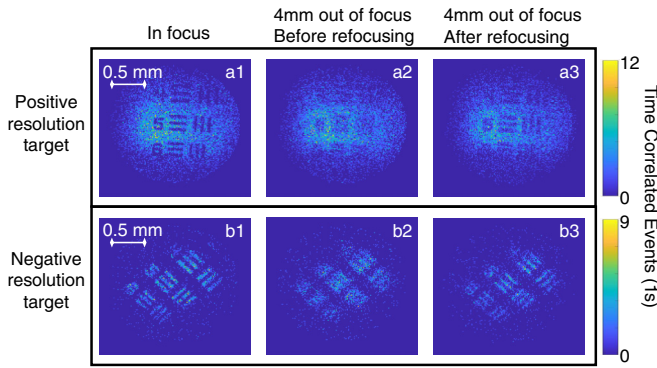


FIG. 5. A positive resolution target is shown placed in focus in a1, placed 4 mm out of focus in a2 and refocused in a3 with 1-s data-acquisition time. The corresponding images for a negative resolution target are shown in b1–b3.

afforded by quantum enhancements [38] to manifest in improved imaging in future work.

*Outlook.* Our proof-of-principle QCPI setup produces high-visibility refocused images with a data-acquisition time of just 30 s. This is comparable with the latest classical CPI demonstration which employs thermal light that is significantly brighter [39]. However, a significant goal for this technique, and many other quantum-enhanced imaging techniques, is to achieve real-time imaging for which integration times of 1 s or lower are required. With this goal

in mind, we show in Fig. 5 a refocused image with just 1-s integration time. Although the image is noisier than when integrated for 30 s, the features can clearly be seen showing that real-time imaging and refocusing is possible with this system.

Improved image quality in real-time QCPI can be expected with improved future camera development and, indeed, there are two potential routes for improving this with existing technology. The first is to improve the temporal resolution of the camera system which will, in turn, improve the  $g^{(2)}$  of the quantum source and, thus, reduce noise. The temporal resolution of our system is approximately 7 ns, giving our SPDC source a measured  $g^{(2)} \approx 5$ , recent work has demonstrated temporal resolution of the same camera system at the subnanosecond level [40], although not yet with quantum light. With this modification, it would be possible to increase the temporal resolution, and, in turn, the  $g^{(2)}$  by an order of magnitude. The second improvement would be to switch the degenerate wavelength of the SPDC source to 710 nm, another commonly used SPDC wavelength where photocathode in the image intensifier with double the quantum efficiency are available (30–40% compared to 15–20% at 810 nm). With both these improvements in place, we would expect the image visibility to increase by an order of magnitude compared to Fig. 5 for the same integration time. Alternatively, images of the same quality could be produced at around 10 fps.

*Acknowledgments.* We are grateful to P. Bustard, F. Bouchard, K. Heshami, D. Guay, and D. Moffatt for technical support and stimulating discussions. This work was partly supported by Defence Research and Development Canada.

- [1] G. Brida, M. Genovese, and I. Ruo Berchera, Experimental realization of sub-shot-noise quantum imaging, *Nat. Photonics* **4**, 227 (2010).
- [2] T. Gregory, P.-A. Moreau, E. Toninelli, and M. J. Padgett, Imaging through noise with quantum illumination, *Sci. Adv.* **6**, eaay2652 (2020).
- [3] J. Zhao, A. Lyons, A. C. Ulku, H. Defienne, D. Faccio, and E. Charbon, Quantum light detection and ranging, [arXiv:2105.07169](https://arxiv.org/abs/2105.07169).
- [4] M. J. Padgett and R. W. Boyd, An introduction to ghost imaging: Quantum and classical, *Philos. Trans. R. Soc. A* **375**, 20160233 (2017).
- [5] G. Zheng, C. Kolner, and C. Yang, Microscopy refocusing and dark-field imaging by using a simple led array, *Opt. Lett.* **36**, 3987 (2011).
- [6] G. Zheng, R. Horstmeyer, and C. Yang, Wide-field, high-resolution fourier ptychographic microscopy, *Nat. Photonics* **7**, 739 (2013).
- [7] R. Schulein, M. Daneshpanah, and B. Javidi, 3d imaging with axially distributed sensing, *Opt. Lett.* **34**, 2012 (2009).
- [8] E. H. Adelson and J. Y. A. Wang, Single lens stereo with a plenoptic camera, *IEEE Trans. Pattern Anal. Machine Intelligence* **14**, 99 (1992).
- [9] <https://raytrix.de/>
- [10] X. Xiao, B. Javidi, M. Martinez-Corral, and A. Stern, Advances in three-dimensional integral imaging: Sensing, display, and applications, *Appl. Opt.* **52**, 546 (2013).
- [11] M. Martínez-Corral and B. Javidi, Fundamentals of 3d imaging and displays: A tutorial on integral imaging, light-field, and plenoptic systems, *Adv. Opt. Photonics* **10**, 512 (2018).
- [12] O. Matoba, E. Tajahuerce, and B. Javidi, Real-time three-dimensional object recognition with multiple perspectives imaging, *Appl. Opt.* **40**, 3318 (2001).
- [13] S. Kishk and B. Javidi, Improved resolution 3d object sensing and recognition using time multiplexed computational integral imaging, *Opt. Express* **11**, 3528 (2003).
- [14] J.-S. Jang and B. Javidi, Three-dimensional integral imaging of micro-objects, *Opt. Lett.* **29**, 1230 (2004).
- [15] M. Levoy, R. Ng, A. Adams, Matthew Footer, and Mark Horowitz, Light field microscopy, *ACM Trans. Graphics* **25**, 924 (2006).
- [16] R. Prevedel, Y.-G. Yoon, M. Hoffmann, N. Pak, G. Wetzstein, S. Kato, T. Schrödel, R. Raskar, M. Zimmer, E. S. Boyden, and A. Vaziri, Simultaneous whole-animal 3d imaging of neuronal activity using light-field microscopy, *Nat. Methods* **11**, 727 (2014).
- [17] T. W. Fahringer, K. P. Lynch, and B. S. Thurow, Volumetric particle image velocimetry with a single plenoptic camera, *Meas. Sci. Technol.* **26**, 115201 (2015).
- [18] E. M. Hall, B. S. Thurow, and D. R. Guildenbecher, Comparison of three-dimensional particle tracking and sizing using plenoptic imaging and digital in-line holography, *Appl. Opt.* **55**, 6410 (2016).

- [19] Y. Lv, R. Wang, H. Ma, X. Zhang, Y. Ning, and X. Xu, Su-giep4-09: Method of human eye aberration measurement using plenoptic camera over large field of view, *Med. Phys.* **43**, 3679 (2016).
- [20] C. Wu, J. Ko, and C. C. Davis, Using a plenoptic sensor to reconstruct vortex phase structures, *Opt. Lett.* **41**, 3169 (2016).
- [21] C. Wu, J. Ko, and C. C. Davis, Imaging through strong turbulence with a light field approach, *Opt. Express* **24**, 11975 (2016).
- [22] A. Orth, M. Ploschner, E. R. Wilson, I. S. Maksymov, and B. C. Gibson, Optical fiber bundles: Ultra-slim light field imaging probes, *Sci. Adv.* **5**, eaav1555 (2019).
- [23] M. D'Angelo, F. V. Pepe, A. Garuccio, and G. Scarcelli, Correlation Plenoptic Imaging, *Phys. Rev. Lett.* **116**, 223602 (2016).
- [24] F. V. Pepe, F. Di Lena, A. Garuccio, G. Scarcelli, and M. D'Angelo, Correlation plenoptic imaging with entangled photons, *Technologies* **4**, 17 (2016).
- [25] F. Di Lena, F. V. Pepe, A. Garuccio, and M. D'Angelo, Correlation plenoptic imaging: An overview, *Appl. Sci.* **8**, 1958 (2018).
- [26] F. V. Pepe, F. Di Lena, A. Mazzilli, E. Edrei, A. Garuccio, G. Scarcelli, and M. D'Angelo, Diffraction-Limited Plenoptic Imaging with Correlated Light, *Phys. Rev. Lett.* **119**, 243602 (2017).
- [27] F. Di Lena, G. Massaro, A. Lupo, A. Garuccio, F. V. Pepe, and M. D'Angelo, Correlation plenoptic imaging between arbitrary planes, *Opt. Express* **28**, 35857 (2020).
- [28] D. G. England, B. Balaji, and B. J. Sussman, Quantum-enhanced standoff detection using correlated photon pairs, *Phys. Rev. A* **99**, 023828 (2019).
- [29] T. Aidukas, P. C. Konda, A. R. Harvey, M. J. Padgett, and P.-A. Moreau, Phase and amplitude imaging with quantum correlations through fourier ptychography, *Sci. Rep.* **9**, 10445 (2019).
- [30] A. Nomerotski, Imaging and time stamping of photons with nanosecond resolution in timepix based optical cameras, *Nucl. Instrum. Methods Phys. Res., Sect. A* **937**, 26 (2019).
- [31] <https://www.amscins.com/tpx3cam/>
- [32] D. N. Klyshko, The effect of focusing on photon correlation in parametric light scattering, *Zh. Eksp. Teor. Fiz.* **94**, 82 (1988).
- [33] See Supplemental Material at <http://link.aps.org/supplemental/10.1103/PhysRevA.105.L011701> for extra results and details on the experiment.
- [34] S. K. Nayar and Y. Nakagawa, Shape from focus, *IEEE Trans. Pattern Anal. Machine Intell.* **16**, 824 (1994).
- [35] K. Morimoto, A. Ardelean, M.-L. Wu, A. C. Ulku, I. M. Antolovic, C. Bruschini, and E. Charbon, Megapixel time-gated spad image sensor for 2d and 3d imaging applications, *Optica* **7**, 346 (2020).
- [36] I. Ruo Berchera and I. P. Degiovanni, Quantum imaging with sub-poissonian light: Challenges and perspectives in optical metrology, *Metrologia* **56**, 024001 (2019).
- [37] P.-A. Moreau, E. Toninelli, T. Gregory, and M. J. Padgett, Imaging with quantum states of light, *Nat. Rev. Phys.* **1**, 367 (2019).
- [38] M. Genovese, Real applications of quantum imaging, *J. Opt.* **18**, 073002 (2016).
- [39] G. Massaro, D. Giannella, A. Scagliola, F. Di Lena, G. Scarcelli, A. Garuccio, F. V. Pepe, and M. D'Angelo, Light-field microscopy with correlated beams for extended volumetric imaging at the diffraction limit, [arXiv:2110.00807](https://arxiv.org/abs/2110.00807).
- [40] A. Nomerotski, P. Stankus, A. Slosar, S. Vintskevich, S. Andrews, G. Carini, D. Dolzhenko, D. England, E. Figueroa, S. Gera, J. Haupt, S. Herrmann, D. Katramatos, M. Keach, A. Parsells, O. Saira, J. Schiff, P. Svihra, T. Tsang, and Y. Zhang, in *Quantum-Assisted Optical Interferometers: Instrument Requirements*, edited by P. G. Tuthill, A. Mérand, and S. Sallum, Optical and Infrared Interferometry and Imaging VII Vol. 11446 (SPIE, Bellingham, WA, 2020), pp. 290–306.